Biochip-PUF: Physically Unclonable Function for Microfluidic Biochips

Navajit Singh Baban, Ajymurat Orozaliev, and Yong-Ak Song
Division of Engineering
New York University Abu Dhabi, Abu Dhabi, UAE.
Email:{nsb359, ao1217, and rafael.song}@nyu.edu

Urbi Chatterjee

Department of Computer Science and Engineering
Indian Institute of Technology Kanpur, India.

Email: urbic@cse.iitk.ac.in

Sankalp Bose

Department of Chemical Engineering Indian Institute of Technology Kharagpur, India.

Sukanta Bhattacharjee
Department of Computer Science and Engineering
Indian Institute of Technology Guwahati, India.
Email: sukantab@iitg.ac.in

Ramesh Karri

Department of Electrical and Computer Engineering New York University, New York, USA. Email: rkarri@nyu.edu Krishnendu Chakrabarty
School of Electrical, Computer and Energy Engineering
Arizona State University, Tempe, AZ, USA.
Email: Krishnendu.Chakrabarty@asu.edu

Abstract—Flow-based microfluidic biochips (FMBs) have microvalves as key components. The physical characteristics of the microvalves vary instance-to-instance due to the inherent variability of numerous fabrication parameters. In this work, we leverage this unclonable, unpredictable instance-specific behavior and propose physically unclonable functions (PUFs) for FMBs, namely Biochip-PUFs (Bio-PUFs in short). We utilize variability in the microvalve membrane deflection response associated with the actuation pressure challenge to be our Bio-PUF parameter. Based on the distributions of the parameters measured on actual FMBs, we complement our Bio-PUF measurements via simulations of the FMB's microvalves in Comsol Multiphysics. Furthermore, we present a scheme based on the transient response of the microvalve actuation to augment the Bio-PUF authentication. The major advantage of this scheme is that we do not need any additional hardware to generate/implement the PUF module. The biochip itself can act as PUF instances while continuing to operate in normal functioning mode.

I. INTRODUCTION

In late 2019, severe acute respiratory syndrome coronavirus 2 (SARS-CoV-2) disease (COVID-19) emerged as a public health emergency of global concern. Molecular diagnostic tests have been used to control this outbreak. Researchers are trying to invent low-cost and accurate molecular diagnostic kits for virus detection [1]–[3]. These methods, collectively known as microfluidics, have been used so far in medical diagnostics, DNA analysis, cell analysis, and drug discovery.

A microfluidic platform or microfluidic biochip comprises a set of microfluidic devices that can be combined seamlessly to create a miniaturized platform for fundamental bench-top laboratory operations such as fluid transportation, metering, and mixing. Microfluidic biochip components such as microreaction chambers, microfluidic channels, and microvalves are integrated with each other forming an integrated fluidic circuit (IFC) into a single chip [4]. Additionally, custom software is used to regulate them automatically, thereby eliminating the necessity of using a cumbersome experimental setup.

Thus, microfluidic platforms enable the miniaturization, integration, automation, and parallelization of biological assays. They have advantages over traditional laboratory procedures in terms of high throughput, low cost, ease of controlling, and reliability [5]. The global microfluidics market size is expected to reach \$44.0 billion by 2025 from an estimated value of \$15.7 billion in 2020 [6]. Several factors, such as the rising demand for point-of-care testing, technological advancements, and portability through microfluidic chip miniaturization, are driving the market. However, as with most emerging technologies, innovation is prioritized, and security is an afterthought in response to discovered vulnerabilities. For example, \$40 million worth of fake or substandard COVID test kits have already been seized in 77 countries, and 407 people have been arrested in operations carried out from December 2019 to June 2020 [7]. Piracy has become a serious threat undermining the effort to design a proprietary protocol [8]. Hence, there is an urgent need for effective authentication to protect the microfluidics market from counterfeit devices.

Microfluidic biochips are mainly categorized into two types based on the underlying technologies used for their operation: digital microfluidic biochips (DMFBs) and flow-based microfluidic biochips (FMBs) [9]. DMFBs use discrete droplets on an electrode array leveraging the principle of electrowetting-on-dielectric [10], [11], while FMBs manipulate fluid flow in microchannels using microvalves [4].

FMBs allow automated control of fluid flow in picoliter volumes in a network of micro-channels by suitable actuation of pressure-driven microvalves. The microvalve is the basic

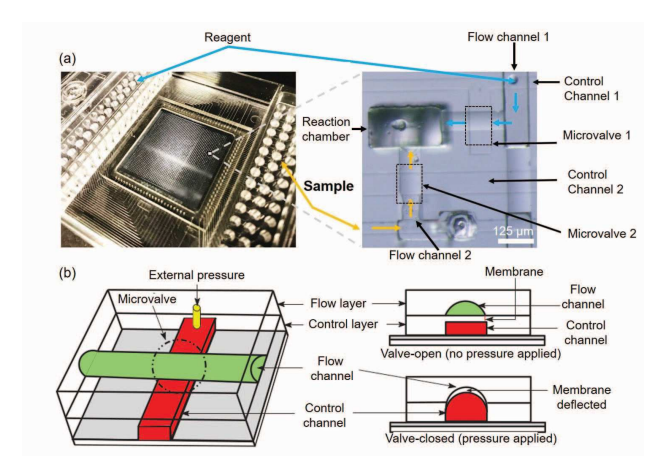


Fig. 1. Microvalves-based FMB. (a) A commercial FMB featuring microfluidic channels, reaction chambers, and microvalves. The bright-field microscopy image displays a reaction chamber linked to the sample and reagent lines through corresponding microfluidic valves. These valves are pneumatically regulated by the control channels. (b) The diagram illustrates the activation of a microvalve via membrane deflection due to by pressure.

primitive of FMBs and it can be considered to be analogous to a transistor in semiconductor electronics [12], [13]. These valves are typically fabricated using Polydimethylsiloxane (PDMS) material [4]. External sources through the microchannels generate continuous flows in this chip, and microvalves are used to precisely control microlevel fluid transportation. By opening/closing the valves, complex fluid handling operations such as mixing, dilution, incubation, transportation, and storage can be performed [14], [15]. Fig. 1(a) shows a commercial FMB for genotyping with 2304 independent reaction chambers connected with microfluidic channels [4]. From one side, sample fluids can be pipetted, while from the other side, reagents can be pipetted. The fluids, after being allowed to flow by the respective microvalves, enter the reaction chamber, where mixing takes place for the subsequent polymerase chain reaction (PCR) cycles [4]. Fig. 1(b) shows a schematic illustrating the microvalve actuation via associated PDMS membrane deflection [16]. Use of PDMS in FMBs has enabled large-scale integration of these valves and paved the way for a transformation from a simple topology with a few channels to an extensive network for practical applications.

In this paper, we focus on microvalve-based FMBs, the valve dynamics of which are determined by their geometry, design complexity, and placement positions in the system. The physical characteristics of these microvalves, such as membrane stiffness, elasticity, and geometry, vary instance-to-instance due to inherent variability associated with the fabrication process. We leverage this unclonable, unpredictable instance-specific system behavior to propose the first-ever physically unclonable functions (PUFs) for FMBs, namely Biochip-PUFs or, Bio-PUFs in short. We utilize variability associated with the microvalve membrane deflection response resulting from the actuation pressure challenge as our Bio-PUF parameter. Based on the distributions of the parameters

measured on actual FMBs, we complement our Bio-PUF measurements via simulations of the micro-valves in Comsol Multiphysics [17].

Furthermore, we present a scheme based on the transient response of the microvalve actuation as an additional feature for the Bio-PUF authentication. An advantage of this scheme is that additional hardware is not needed to implement the PUF. The microvalves serve as PUF instances without interfering with the function of the FMB.

The major contributions of this paper are threefold:

- First, we identify a reliable and repetitive entropy source that can be used as instance-specific behavior of a chip.
- Next, we present a novel candidate Bio-PUF design using the membrane deflection variability in response to the actuation pressure challenge. Experimentally, we demonstrate this property to generate the challenge-response pair of the PUF instance as a signature of the chip for physical authentication of FMBs.
- Finally, we characterize the uniqueness, uniformity, and reliability of Bio-PUFs using Comsol Multiphysics simulations.

The rest of the paper is organized as follows. Section II provides the fundamentals of FMBs and silicon-based PUFs. In Section III, we describe the adversarial model. Experimental results are demonstrated in Section IV. Simulation results are presented and discussed in Section V and discussion Section VI, respectively. Conclusions are presented in Section VII.

II. BACKGROUND

In this section, we give an overview of an FMB and analyze potential variability in the chip that can be used as an entropy source. We also provide an introduction to silicon-based PUFs and the desirable PUF properties.

A. Flow-based Microfluidic Biochip

The fundamental component of an FMB is a microvalve that controls the fluid flow in a network of microchannels. Soft lithography [18]–[20] is used to replicate molding elastomeric materials such as polydimethylsiloxane (PDMS) to fabricate these microvalves. Initially, a photoreactive polymer, referred to as photoresist, is spin-coated on a silicon wafer. A contact mask of molds patterned by using a high-resolution transparency film is kept on top of the photoresist layer and exposed to ultraviolet (UV) light. As a result, the photoresist is illuminated by UV light through the mask.

Subsequently, when the wafer is placed in an organic solvent, the photoresist gets dissolved and removed. Due to the exposure to UV light, the pattern from the mask is engraved into the photoresist. This is considered as the master copy. The height of the polymer structure is controlled by the thickness of the layer of photoresist that is initially spread on the surface of the wafer. Finally, PDMS is spread over the master copy and thermally cured in an oven [4]. The PDMS layer is then discased, and we get the inverse of the original pattern punched on the surface of the master copy.

An FMB consists of two elastomer layers: a flow layer, which consists of channels for liquid flow, and a control layer, which consists of channels that can be pressurized or actuated with fluids (air or liquid) to deflect the microvalve membrane into the flow channel, thereby blocking the flow channel's liquid flow [21]. Channels in both layers are connected to an external pressure source, which generates the pressure to drive liquid flows as well as actuate the microvalves [4].

Due to elastomeric properties of the PDMS, the response of the microvalve depends on the physical properties such as membrane stiffness, height, and fluid resistance in the liquid flows [22]. Additionally, due to variations associated with the fabrication process parameters such as spin coating [23], temperature [24], photolithography etch rate [25], and pressure gradient along the microchannels [16], microvalves showcase different physical properties for different device designs.

The main idea of this work is to leverage these elastomeric properties of the PDMS, and the impact of design complexities as the hardware-intrinsic property of a particular microvalve to generate a PUF signature for the microfluidic device.

B. Silicon-based PUFs

Physically unclonable functions (PUFs) [26], [27] have been proposed as a promising unconventional cryptographic primitive for IC anti-counterfeiting [28], device identification and authentication [29], [30], binding hardware to software platforms [31], secure storage of cryptographic secrets [32], and keyless secure communication [33]. A silicon PUF is an input-output mapping $\gamma: \{0,1\}^n \to \{0,1\}^m$, where the output m-bit output response words are unambiguously identified by both the n-bit input challenge words, and the unclonable, unpredictable (but repeatable) instance-specific system behavior. It is easy to fabricate but practically infeasible to clone, despite the highly precise manufacturing process that produces it. It exploits variation in manufacturing across different dies, wafers, and processes to generate (ideally) unique challengeresponse mapping for each instance as shown in Fig. 2(a). The desirable physical properties of a silicon PUF are:

- **Physical Unclonability** ensures that the PUF instance is easy to fabricate but infeasible to clone.
- **Uniqueness** of the embedded PUF instance provides the capability of uniquely identifying it from a set of PUF instances of the same type, which have gone through the same manufacturing process.
- **Uniformity** of the PUF instance embedded in a chip ensures that the correlations among all possible responses of the PUF over the challenge space are negligible and have high bit entropy.
- **Reliability** of the PUF determines the stability of the PUF responses across ambient factor variations, such as time, temperature, and humidity.
- Tamper-proofness guarantees that any tampering with the PUF instance will not change its behavior.
- Mathematical Unclonability depicts that given a subset of challenge-response pairs of a PUF instance, an adversary cannot build a mathematical model of it.

Several applications of PUFs in the security domain have been proposed, such as "key-less" device authentication and identification, random number generation, intellectual property (IP) protection, and secure protocol design. We briefly discuss below the traditional PUF-based authentication scheme, as shown in Fig. 2(b). It involves two parties, a prover and a verifier, and proceeds as follows:

- Enrollment Phase: In this phase, the PUF instance of the prover is characterized based on a set of challenges, and the responses are stored by the verifier in a Challenge-Response Pair Database (CRPDB) along with the identity of the prover. It is assumed that the enrollment phase is executed in a secure and trusted environment.
- 2) Authentication Phase: Here, the device sends its identity to the verifier that randomly picks an entry from CRPDB of that identity and authenticates the device by characterizing the PUF instance with the challenge, collecting the response, and matching it with the stored response.

Prior work on securing FMBs against IP-theft-based attacks [4] mainly involves watermarking [4], [34] and obfuscation techniques via inserting dummy microvalves in FMBs [22]. Thus far, no work has been done to secure FMBs against IP-theft threats via a PUF-based authentication scheme. Thus, to provide authentication, unclonability, and provenance verification of FMBs, we propose the first-ever device-level scheme to extend the functionality of traditional silicon-based PUFs to FMBs using their microvalves. The objective of this work is to design PUF instances for FMBs that are unlikely to be physically cloned, even though they have been fabricated using the same manufacturing process. Additionally, the PUF signatures across the devices should be unique, uniform, reliable, tamper-proof, and cannot be mathematically modeled.

III. ADVERSARIAL MODEL

The setting assumed is that the cyberphysical microfluidic system (CPMS) consists of a flow-based microfluidic biochip (FMB), an FMB controller, and a trusted third party (TTP) that monitors the executions of FMBs [35] (see Fig. 3). We assume that the TTP can securely store the challenge-response pair database (CRPDB) for every FMB. The TTP is also equipped with a charge-coupled device (CCD) camera.

The FMB controller is responsible for launching a pressuredriven actuation sequence to the FMB's microvalves, which can be controlled by network-based interfaces. The TTP is physically segregated from the controller. Each chip can manipulate fluids for biochemical reactions as instructed in the actuation sequences. On the other hand, it can operate as a PUF and prove its identity to the TTP responsible for authenticating the signature.

At the time of authentication, the FMB is put under the CCD camera, and the challenge (actuation sequence) is applied to it. The FMB is characterized with respect to the challenge, and the response is captured using the camera. If the response is the same as the response stored in the database, the FMB is authenticated. The goal of the adversary is to replace a legitimate FMB with an illegitimate/counterfeit FMB and still

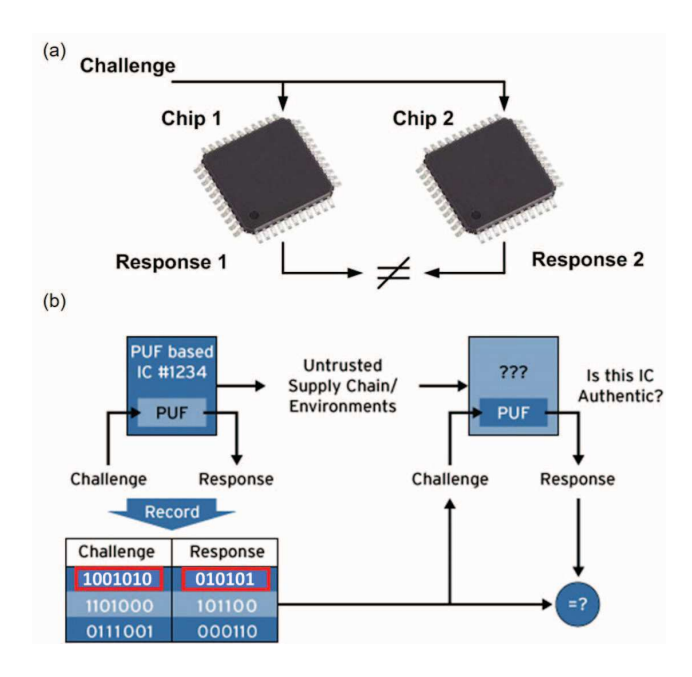


Fig. 2. (a) Physically Unclonable Function. (b) PUF-based Authentication Protocol

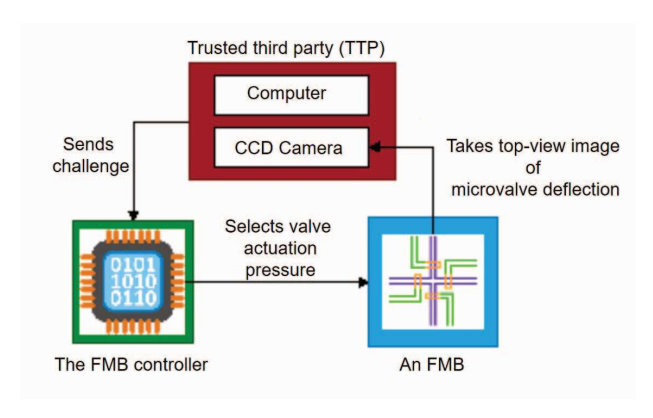


Fig. 3. The setting of a CPMS.

be able to authenticate itself to the TTP. However, for a PUF instance embedded in the FMB, its challenge-response characteristic is an implicit property and thus, unlikely to be reverse-engineered by the adversary.

In the next section, we discuss results on our Bio-PUF primitive and evaluate the variability of the Bio-PUF response with respect to a particular applied pressure challenge.

IV. BIO-PUF EXPERIMENTAL RESULTS

This section describes experimental results to evaluate the variability parameters associated with the Bio-PUF responses. Using a commercial FMB as a reference, we fabricated an FMB whose microvalve dimensions were designed using the reference FMB's valve dimensions, as shown in Fig. 1(a) [4]. Fig. 4(a) shows the schematic of our laboratory-made FMB,

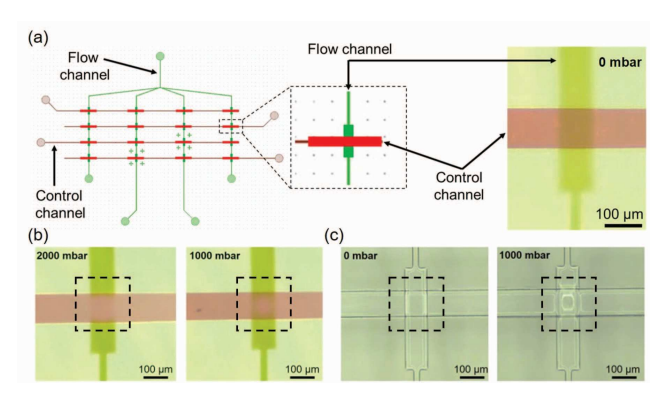


Fig. 4. Bio-PUF Experimental Outcomes: (a) A schematic of our lab-constructed FMB, created using photolithography, PDMS replication, and plasma bonding. The magnified section displays a single microvalve. The bright-field microscopy image exhibits a single microvalve with red and green dyed fluids at a control channel pressure of 0 mbar (valve-on). (b) The microvalve with red (in the flow channel) and green (in the control channel) dyed fluids under a pressure of 2000 mbar, demonstrating a fully closed state. Additionally, the microvalve with dyed fluids presents a partially closed state at 1000 mbar pressure. (c) A microvalve (with no fluids present in the channels) in an open valve state (0 mbar). The microvalve (with no fluids in the channel) in a partially closed state, subjected to a pressure of 1000 mbar."

where the associated image shows a bright-field microscopy image of a single microvalve. Red and green dyed fluids were inserted in the control and flow channels, respectively, to visualize the channel fluids during the microvalve actuation. The valve is in a not-actuated (valve-open) condition, i.e., 0 mbar pressure was applied to the control channel.

We demonstrated experimentally that the increase or decrease of the area in the flow channel, which is a direct function of the valve deflection, has an impact on the intensity of the dyed fluids passing through the channel. Fig. 4(b) shows the fully closed valve condition (valve-off) under 2000 mbar pressure. In comparison, Fig. 4(b) shows a partially closed valve condition under 1000 mbar pressure, where the middle portion of the valve shows an oval-shaped red color surrounded by the green fluid. The red oval is due to the red fluid in the control channel because of the deflected membrane. In comparison, the surrounding green color is due to the remaining green fluids of the flow channel resulting from the partially closed valve condition.

However, for Bio-PUF, it is important not to insert any fluid in the channel as it could potentially contaminate the FMB, making it unfit before actual use. Thus, we tested the microvalves without any fluid to characterize the Bio-PUF response. Fig. 4(c) shows the not-actuated (0 mbar pressure, valve-open) and the actuated (1000 mbar pressure, valve-partially-closed) microvalve with no fluids. The actuated valve shows the middle oval due to the deformed membrane, which contacts the flow channel surface.

Thus, the intensity change associated with the oval formation in the microvalve junction can be directly correlated to the valve deflection. This intensity change, as a result of associated microvalve deflection, can be used to verify the Bio-PUF challenge response through a CCD camera connected

with the bright-field microscope [36].

Fig. 5(a) shows a schematic of our laboratory-made FMB with the microvalves, flow, and control channels. The microvalves are numbered from 1 to 16. To evaluate the effect of membrane thickness on valve deflection, we designed 8 out the 16 valves with a membrane thickness 100% higher (40 μ m thick membrane) than the rest valves (20 μ m thick membrane).

Fig. 5(b) shows the bright-field microscopy images of the microvalves from 1 to 12 of the laboratory-made FMB. For the applied pressure of 1000 mbar, it can be seen in Fig. 5(b) that the thicker membrane valves deflect less as compared to the normal valves. This is evident from the smaller ovals formed, which was due to the thicker membrane valves compared to the normal ones. Thus, for a given pressure, we recorded that the valve deflection decreases with higher membrane thickness. The aspect of membrane thickness-dependent microvalve response inherently adds to the variability associated with the Bio-PUF. This is because a thickness variation is likely and inadvertently to be incorporated into the valve membrane due to the associated spin-coating fabrication process [23].

We performed a variability study on the Bio-PUF by quantifying and evaluating responses of microvalves from two different FMBs. All the valves were subjected to 1000 mbar pressure as the actuation challenges. The responses were quantified using the ImageJ image processing software. Fig. 5(c) shows the non-actuated (0 mbar pressure) and actuated (1000 mbar pressure) cases, as seen under the bright-field microscope. We converted the image to a grayscale image and analyzed the region of interest (ROI) by drawing a rectangle containing the microvalve portion, as seen in Fig. 5(c).

To analyze the Bio-PUF variability in response to the actuation challenge of 1000 mbar pressure, we calculated the mean gray value for four cases with five samples each: FMB 1, 20 µm thick membrane from batch 1, FMB 2, 20 µm thick membrane from batch 2, FMB 1, 40 µm thick membrane from batch 1, and FMB 2, 40 µm thick membrane from batch 2. The calculated mean gray value was divided by the area of the corresponding ROI rectangle to normalize the responses. Fig. 5(d) shows the obtained results, which illustrate considerable variability of the microvalve responses within a single FMB as well as between different batch FMBs for a given actuation pressure challenge (1000 mbar). The variability within a single FMB's microvalve responses can be estimated through the corresponding standard deviation.

For example, we recorded the standard deviation for FMB 1 with the 20 μ m thick membrane to be 0.0014 gray-values/ μ m³, which is 5.1% of the corresponding mean value (0.028 gray-values/ μ m³). On the other hand, for FMB 2 with the 20 μ m thick membrane, the mean and standard deviation were 0.032 gray-values/ μ m³ and 0.008 gray-values/ μ m³, respectively. Notably, we recorded the standard deviation of FMB 2 with the 20 μ m thick membrane to be approximately 5-fold higher (25%) than the standard deviation for FMB 1, showing the variability between different batch FMBs. Similar results were obtained for the 40 μ m thick membrane valves, too, as seen in 5(d).

In summary, we recorded considerable variability with

respect to the Bio-PUF responses for an actuation pressure challenge within a single FMB and between different batch FMBs. These variations can be attributed to the inherent differences related to the fabrication process parameters such as spin coating [23], temperature [24], photolithography etch rate [25], and pressure gradient along the microchannels [16]. We performed uniqueness, uniformity, and reliability studies for the Bio-PUF using microvalve simulations results, as discussed in the next section.

V. BIO-PUF SIMULATION RESULTS

The microvalves in an FMB can be used to produce a unique signature due to the inherent randomness induced at the time of the manufacturing process. Since the valve technology is used for components such as peristaltic pumps, microfluidic multiplexers, storage cells, etc., enabling hardware fingerprinting of the chip provides an added advantage to the microfluidic large-scale integration (mLSI) system. Below, we provide details on the microvalve actuation simulation. We mainly focus on microvalve membrane deflection under different membrane thickness and temperature conditions to evaluate its impact on the Bio-PUF's uniqueness, uniformity, and reliability properties.

Mechanical deformations of the microvalve (Fig. 6(a)) with defined configurations were computed using Comsol Multiphysics, which is a commercially available finite element analysis package. Two-dimensional computational models with the membrane thicknesses ranging from $20~\mu m$ to $30~\mu m$ were constructed for the microvalve.

The material considered for the valve was PDMS. To model the PDMS microvalve's hyperelastic material properties, we adopted the Neo-Hookean hyperelastic model [37] (Lamé constant $\mu=678.6$ kPa; Lamé constant $\lambda=1.0714$ MPa) with the density $\rho=920$ kg/m³. A semi-elliptical flow channel was selected with a depth and width of $10~\mu m$ and $50~\mu m$, respectively. A triangular physics-controlled mesh was used for meshing the microvalve model. The pressure applied to the top surface boundary ranged from 0-300 mbar for simulating the deformation. A fixed boundary condition was applied to all the edges except for the pressure-boundary condition edge.

Fig. 6(a) shows the fully open valve condition, i.e., when no pressure was applied on the PDMS membrane for a microvalve with a $20~\mu m$ membrane thickness. When we applied pressure of 150~mbar, the valve got partially deflected (see Fig. 6(c)). After a higher pressure of 300~mbar was applied, the microvalve got fully closed, as shown in Fig. 6(c). Using the simulation, we were able to record microvalve actuation responses for different membrane thicknesses under varying pressure and conditions.

In the next section, we present the obtained simulation results to discuss the uniqueness, uniformity, reliability, and transient response properties of the Bio-PUF with respect to the variability associated with the microvalve membrane deflection.

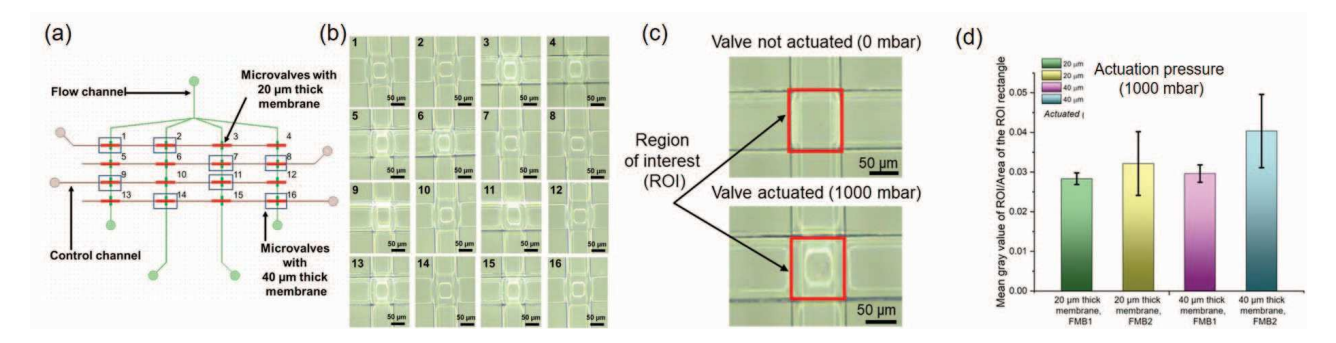


Fig. 5. Experimental results for Bio-PUF variability: (a) A schematic showing the microvalves, flow and control channels. The microvalves are numbered from 1 to 16. The higher membrane valves can be identified with the surrounded rectangles. (b) Bright-field microscopy images of different microvalves from 1 to 12. (c) A bright-field microscopy image of a single microvalve in non-actuated (0 mbar) and actuated condition (1000 mbar). (d) Normalized mean gray values for 20 different actuated microvalves classified into four cases, five samples each (n=5): FMB 1, 20 μ m thick membrane from batch 1, FMB 2, 20 μ m thick membrane from batch 2, FMB 1, 40 μ m thick membrane from batch 2. The error bar represents standard deviation

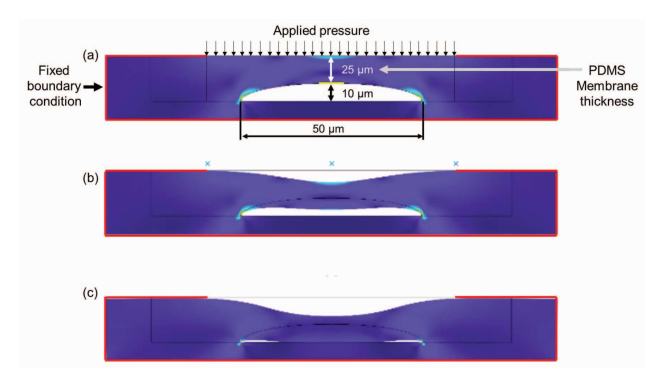


Fig. 6. Microvalve membrane (25 μ m thick) deflection simulation in COMSOL Multiphysics: a) Fully open condition at 0 mbar pressure, b) Partially closed condition at 150 mbar pressure. c) Fully closed condition at at 300 mbar pressure.

VI. DISCUSSION

In the following sub-sections, we discuss the uniqueness, uniformity, and reliability properties of the Bio-PUF as a function of the flow channel's cross-sectional area variability arising from the associated microvalve membrane deflection.

A. Uniqueness

For simulations, we used the microvalve membrane thickness ranging from 22 μ m to 30 μ m with a step-size interval of 2 μ m. We chose the step-size considering the 5% standard deviation, as seen in Fig. 5(d). For instance, if we consider a 40 μ m valve membrane thickness and 5% standard deviation, the resulting step-size (5% of 40 μ m) is equal to 2 μ m. The pressure applied to the valve membrane were varied from 0 mbar to 300 mbar with a step-size interval of 50 mbar.

Using this simulation procedure, we calculated the normalized (with respect to the not-actuated condition) flow channel's cross-sectional area as follows:

• An image of the deflected valve was recorded and saved.

- The image was cropped to include the elliptical valve in a rectangular frame. The image was converted to Grayscale.
- Next, we count the number of white pixels in the image, which denotes the area of the flow channel after deflection.
- The normalized flow channel's cross-sectional area was calculated by dividing the area of the flow channel after deflection with that before deflection at 0 mbar.
- Next, all these area measurements for the valves of varying heights were saved in a csv file.
- The data frames were merged into one, each column corresponds to data for a particular height of the control layer. Finally, the normalized flow channel's crosssectional area variance was calculated for each column.

Fig. 7 shows the normalized flow channel's cross-sectional area variance for each microvalve membrane thickness to evaluate the Bio-PUF's uniqueness properties. The plot signifies that the microvalve deflection behavior varies significantly with respect to different membrane thickness. These variabilities can be leveraged to generate unique challenge-response pairs, which can exclusively be identified with the help of CCD camera linked with a bright-field microscope, assuming that the microscope is sensitive enough to detect these minute microvalve membrane variations.

B. Uniformity

For an effective Bio-PUF authentication, the responses generated for different challenges from an FMB's microvalves should be uniform. In our setup, the challenge is the varying pressures, and the response is the change in the flow channel's cross-sectional area applying the pressure.

We experimentally demonstrate the uniformity by plotting the normalized (with respect to the not-actuated condition) flow channel's cross-sectional area versus varied actuation pressures for $20~\mu m$ and $40~\mu m$ microvalve membrane thicknesses, as seen in Fig. 8(a) and Fig. 8(b), respectively. Both

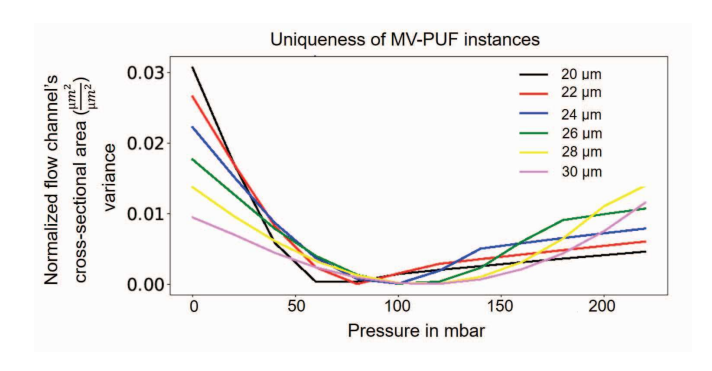


Fig. 7. Uniqueness of the microvalve deflection response: normalized flow channel's cross-sectional area variance vs. varied actuation pressures. Normalization was done with respect to the flow channel's cross-sectional area at 0 mbar pressure (not-actuated condition).

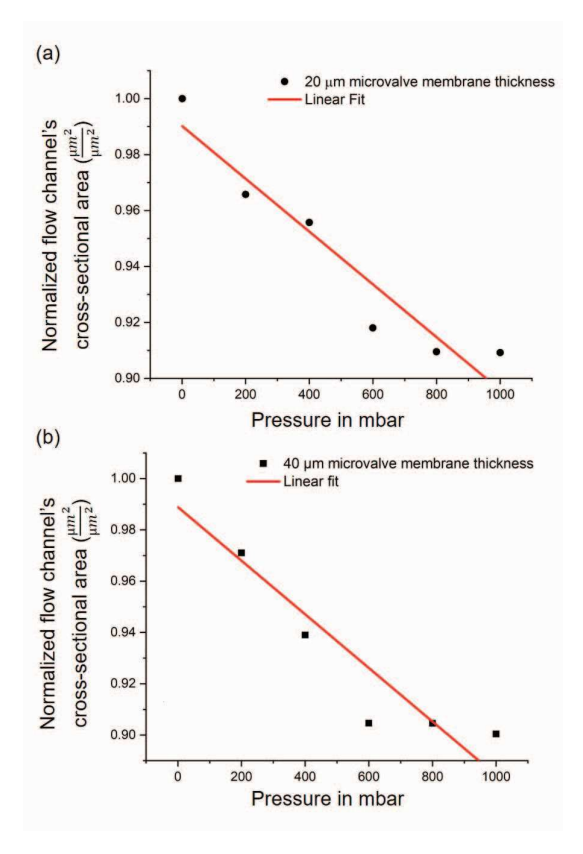


Fig. 8. Experimental results for uniformity evaluation: (a) normalized flow channel's cross-sectional area versus varied actuation pressures response for a 20 μm microvalve membrane thickness. (b) normalized flow channel's cross-sectional area versus varied actuation pressures response for a 40 μm microvalve membrane thickness. Normalization was done with respect to the flow channel's cross-sectional area at 0 mbar pressure (not-actuated condition)

plots show distinct variations in the actuation response with respect to varying pressures.

Furthermore, we analyze uniformity based on the simulation results. Fig. 9 shows the normalized flow channel's cross-sectional area vs. applied pressure simulation response for a 30

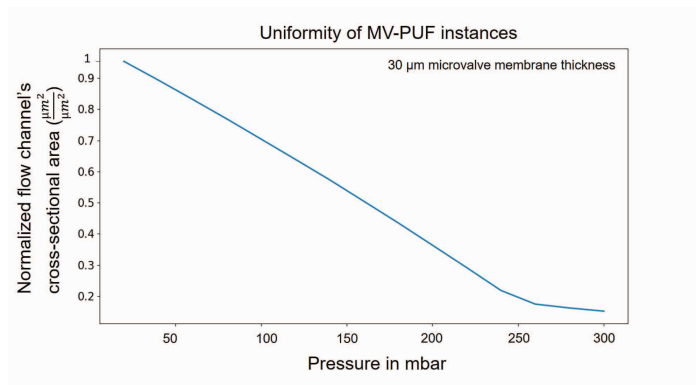


Fig. 9. Normalized flow channel's cross-sectional area vs. varied actuation pressures. Normalization was done with respect to the flow channel's cross-sectional area at 0 mbar pressure (not-actuated condition).

µm microvalve membrane thickness. The plot shows a discrete variation in the actuation response with respect to varying pressure similar to the experimental results. This confirms a good agreement between the simulations and experiments. Thus, the Bio-PUF scheme can provide an effective authentication scheme based on the uniformity of the microvalve actuation response with respect to varying pressure challenges.

C. Reliability

An important aspect of a PUF is its reliability. It quantifies how effective a PUF is in reproducing the response bits under different operating conditions. We simulated the Bio-PUF instances with respect to temperature ranging from $-20^{\circ}\mathrm{C}$ to $80^{\circ}\mathrm{C}$. We used the heat transfer module for advanced simulation in Comsol Multiphysics and entered the temperature range as specified under the sub-categories. Using the heat transfer module based Comsol model, we analyzed the impact of temperature variation on the PDMS material and, in turn, the behavioral changes in the valve deflection. Fig. 10 shows a plot between normalized flow channel's cross-sectional area versus varied pressures at different temperatures. Normalization was done with respect to the flow channel's cross-sectional area at 0 mbar pressure (not-actuated condition).

The results in Fig. 10 show a nominal variation in the normalized flow channel's cross-sectional area for the pressure ranging from 0 to 125 mbar at room temperatures (20°C to $25^{\circ}\mathrm{C}$). However, considerable variation can be seen in the normalized flow channel's cross-sectional area at higher temperature (40°C and above) and higher pressure (150 mbar and above). The reason behind this temperature-dependent valve response could be attributed to Neo-Hookean hyperelastic model's temperature dependence [37].

Therefore, according to the simulation results, the temperature and the pressure at which a microvalve operates can affect its membrane deflection, thereby compromising the reliability parameter. Thus, it is important to maintain the desired microvalve temperature during Bio-PUF authentication.

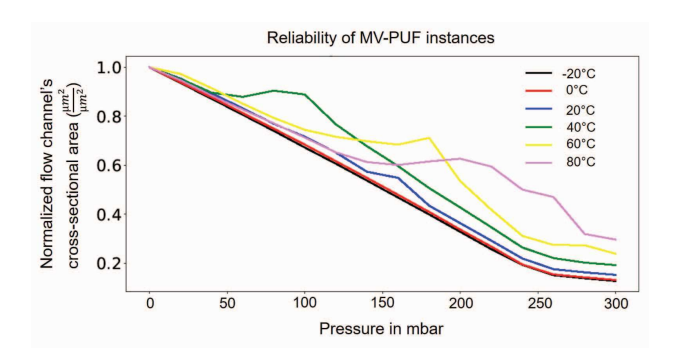


Fig. 10. Normalized flow channel's cross-sectional area versus varied pressures at different temperatures. Normalization was done with respect to the flow channel's cross-sectional area at 0 mbar pressure (not-actuated condition).

D. Transient Response

We present an algorithm to generate challenge-response pairs, which involves transient responses of a microvalve actuation. The algorithm considers transient parameters such as attachment, closure, and restoration times of the valve actuation under different driving pressures [38]. A time-lapsed image of the membrane deflection can be used to calculate these parameters and be considered as the PUF response for a particular microvalve to authenticate the FMB.

We define the terms: attachment time, closure time, and restoration time as follows:

- The attachment time of a microvalve is the time required for a deflecting membrane under a driving pressure to first contact with the bottom of the underlying flow channel.
- The closure time is the period that a microvalve takes to completely block the flow channel.
- The restoration time is the duration required for a fully deflected membrane to return to its open state after the driving pressure is released.

To characterize transient response, the external challenge applied to the PUF instance is the driving pressure. We can apply a step-signal to an electro-fluidic valve to switch the driving pressures for the microvalve actuation or de-actuation while the signal is simultaneously fed also to a light-emitting diode (LED) for visualizing the command. We can capture both illumination and deformation through a digital camera. The time-lapsed image of the membrane deflection can be used to calculate the attachment, closure, and restoration time and be considered as the PUF response for a particular microvalve. As an example of the working principle, we provide timelapsed images of membrane deflections, as seen in Fig. 11.

Fig. 11(a) and Fig. 11(b) show time-lapsed images of membrane deflections during pressurized actuation (1000 mbar) and release, respectively. The recorded time corresponding to the time-lapsed images can be used to calculate attachment, closure, and restoration time to populate CRPDB.

Notably, it is critical to define the starting time point of an actuation sequence for the Bio-PUF authentication. This is because there could possibly be a mismatch in the actuation

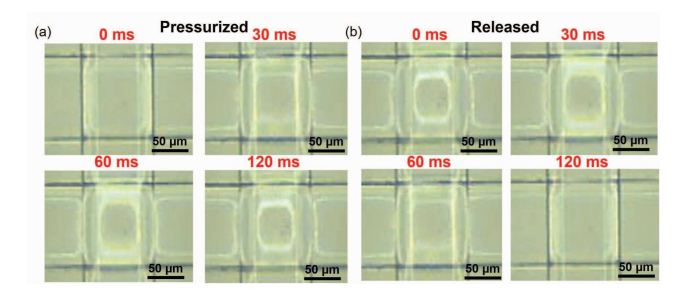


Fig. 11. Transient response of a microvalve actuation. Time-lapsed images of the 40 µm thick membrane's deflections during (a) pressurized actuation (1000 mbar) and (b) release.

starting time during authentication with the corresponding starting time that was used during the CRPDB building procedure. During the Bio-PUF authentication phase, the FMB's microvalve response is needed to be matched with the responses stored in CRPDB. However, if the actuation starting point is not distinctly defined during the authentication done by the TTP, then there will be a mismatch between the compared microvalve responses, thereby leading to an authentication failure. Thus, it is important to impart a closed-loop automation system [39] to the FMB and its auxiliary instruments, such as CCD cameras, microscopes, etc., during the Bio-PUF authentication and the CRPDB building procedure. This addition will eliminate the time mismatch between the TTPobtained responses versus the responses stored in CRPDB, making the Bio-PUF authentication error-free. Generating the challenge and transient response is described in Algorithm 1.

From the above discussion, we conclude that the microvalves in an FMB can not only operate in a normal functioning mode, but it can also provide hardware fingerprinting capability during an authentication mode.

Algorithm 1 Calculate transient response

Capture the reset image I_{reset} of valve ind in 0 mbar;

 T_{start} =current_time;

Apply pressure to the valve until it first contact with the bottom of the underlying flow channel;

Capture the image I_{attach} of the valve ind and the pressure value P_{attach} ;

 $T_{attachment} = current_time - T_{start};$

Apply pressure to the value until it completely blocks the flow channel;

Capture the image $I_{closure}$ of the valve ind and the pressure value $P_{closure}$;

 $T_{closure} = current_time - T_{start};$ $new_start_time = current_time;$

Release pressure to the value until it completely returns to the reset phase;

 $T_{restoring} = current_time - new_start_time;$

return Challenge: $\{ind, I_{reset}, I_{attach}, I_{closure}, P_{attach}, \}$ $P_{closure}\};$

return Response: { $T_{attachment}$, $T_{closure}$, $T_{restoring}$ };

VII. CONCLUSION

We have presented the first-ever microvalve-based physically unclonable functions (Biochip-PUFs or, Bio-PUFs in short) for the physical authentication of FMBs. We have utilized variability in the challenge-response pair associated with the membrane deflections to design the Bio-PUF. We have demonstrated the Bio-PUF measurements via experiments using fabricated FMB devices and simulations of the microvalves using the Comsol Multiphysics finite element analysis package. Using benchtop techniques, we have evaluated the variability associated with the Bio-PUF responses with respect to a specific actuation pressure challenge, given that the fabrication process parameters for the PUF instances are the same for all fabricated FMBs. The experimental results recorded a considerable variability in the Bio-PUF responses within an FMB and among different batch FMBs. We have evaluated the uniqueness, uniformity, and reliability properties based on the Bio-PUF instance's membrane deflection variability to validate the proposed Bio-PUF concept. Furthermore, we have presented a scheme to compute the Bio-PUF transient response in terms of attachment, closure, and restoration time under different static pressures for FMB authentication. A key advantage of this scheme is that we do not need any additional hardware to generate/implement the PUF module. The chip itself works as a PUF instance while continuing to operate in its normal functioning mode.

VIII. ACKNOWLEDGEMENT

We thank New York University Abu Dhabi's Core Technology Platform (CTP) for help and access to the microscopy and the clean room microfabrication set up. Karri was supported in part by NSF award 2049311 and Chakrabarty was supported in part by NSF under grant no. 2049335.

REFERENCES

- [1] N. Farshidfar and S. Hamedani, "The potential role of smartphonebased microfluidic systems for rapid detection of COVID-19 using saliva specimen," *Molecular Diagnosis & Therapy*, vol. 24, 2020.
- [2] L. E. Lamb, S. N. Bartolone, E. Ward, and M. B. Chancellor, "Rapid detection of novel coronavirus/severe acute respiratory syndrome coronavirus 2 (sars-cov-2) by reverse transcription-loop-mediated isothermal amplification," *PLOS ONE*, vol. 15, no. 6, pp. 1–15, 2020.
- [3] "Breathtaking: New covid-19 pcr test based on exhaled breath indicates infectiousness," 2023. [Online]. Available: https://www.imec-int.com/en/articles/breathtaking-new-covid-19-pcr-test-based-exhaled-breath-indicates-infectiousness
- [4] N. S. Baban, S. Saha, A. Orozaliev, J. Kim, S. Bhattacharjee, Y. Song, R. Karri, and K. Chakrabarty, "Structural attacks and defenses for flow-based microfluidic biochips," *IEEE Trans. Biomed. Circuits Syst.*, vol. 16, no. 6, pp. 1261–1275, 2022.
 [5] T.-M. Tseng, "Design automation for continuous-flow microfluidic
- [5] T.-M. Tseng, "Design automation for continuous-flow microfluidic biochips," Ph.D. dissertation, Technical University Munich, 2017.
- [6] Markets and Markets, "Microfluidics market by product (devices, components (chips, sensors, pump, valves, and needles), application (ivd [poc, clinical, veterinary], research, manufacturing, therapeutics), end user and region global forecast to 2025," 2020. [Online]. Available: https://www.marketsandmarkets.com/Market-Reports/microfluidics-market-1305.html
- [7] "Fake covid-19 kits seized in international trafficking crackdown from 77 countries," july 2020. [Online]. Available: https://www.ndtv.com/world-news/coronavirus-fake-covid-19-kits-seized-in-international-trafficking-crackdown-from-77-countries-2267147

- [8] S. S. Ali, M. Ibrahim, J. Rajendran, O. Sinanoglu, and K. Chakrabarty, "Supply-chain security of digital microfluidic biochips," *Computer*, vol. 49, no. 8, pp. 36–43, 2016.
- [9] S. Mohammed, S. Bhattacharjee, Y.-A. Song, K. Chakrabarty, and R. Karri, Security of Biochip Cyberphysical Systems. Springer, 2022.
- [10] J. Tang, R. Karri, M. Ibrahim, and K. Chakrabarty, "Securing digital microfluidic biochips by randomizing checkpoints," in *International Test Conference (ITC)*, 2016, pp. 1–8.
- [11] T.-C. Liang, K. Chakrabarty, and R. Karri, "Programmable daisychaining of microelectrodes for IP protection in meda biochips," in *International Test Conference (ITC)*, 2019, pp. 1–10.
- [12] S. Potluri, P. Pop, J. Madsen, and A. Schneider, "Microfluidic valve," 2018, wO2018104516; B01L3/00; F16K99/00.
- [13] P. Pop, W. Minhass, and J. Madsen, Microfluidic very large scale integration (VLSI): modeling, simulation, testing, compilation and physical synthesis. Springer, 2016.
- [14] K. Hu, F. Yu, T. Ho, and K. Chakrabarty, "Testing of flow-based microfluidic biochips: Fault modeling, test generation, and experimental demonstration," *IEEE Transactions on Computer-Aided Design of Integrated Circuits and Systems*, vol. 33, no. 10, pp. 1463–1475, 2014.
- [15] W. H. Minhass, P. Pop, and J. Madsen, "System-level modeling and synthesis of flow-based microfluidic biochips," in *Compilers, Architectures and Synthesis for Embedded Systems (CASES)*, 2011, pp. 225–233.
- [16] N. S. Baban, A. Orozaliev, C. J. Stubbs, and Y.-A. Song, "Biomimicking interfacial fracture behavior of lizard tail autotomy with soft microinterlocking structures," *Bioinspiration & Biomimetics*, vol. 17, no. 3, p. 036002, 2022.
- [17] "Comsol multiphysics," 2023. [Online]. Available https://www.comsol.com/
- [18] D. B. Weibel, W. R. DiLuzio, and G. M. Whitesides, "Microfabrication meets microbiology," *Nature Reviews Microbiology*, vol. 5, pp. 209–218, 2007.
- [19] M. A. Unger, H.-P. Chou, T. Thorsen, A. Scherer, and S. R. Quake, "Monolithic microfabricated valves and pumps by multilayer soft lithography," *Science*, vol. 288, no. 5463, pp. 113–116, 2000.
- [20] J. Goulpeau, D. Trouchet, A. Ajdari, and P. Tabeling, "Experimental study and modeling of polydimethylsiloxane peristaltic micropumps," *Journal of Applied Physics*, vol. 98, p. 044914, 08 2005.
- [21] M. Shayan, S. Bhattacharjee, Y. Song, K. Chakrabarty, and R. Karri, "Desieve the attacker: thwarting IP theft in sieve-Valve-based biochips," in *Design, Automation Test in Europe (DATE)*, 2019, pp. 210–215.
- [22] M. Shayan, S. Bhattacharjee, A. Orozaliev, Y.-A. Song, K. Chakrabarty, and R. Karri, "Thwarting bio-ip theft through dummy-valve-based obfuscation," *IEEE Transactions on Information Forensics and Security*, vol. 16, pp. 2076–2089, 2020.
- [23] S. Askar, C. M. Evans, and J. M. Torkelson, "Residual stress relaxation and stiffness in spin-coated polymer films: Characterization by ellipsometry and fluorescence," *Polymer*, vol. 76, pp. 113–122, 2015.
- [24] M. Liu, J. Sun, and Q. Chen, "Influences of heating temperature on mechanical properties of polydimethylsiloxane," *Sensors and Actuators A: Physical*, vol. 151, no. 1, pp. 42–45, 2009.
- [25] M. L. Fitzgerald, S. Tsai, L. M. Bellan, R. Sappington, Y. Xu, and D. Li, "The relationship between the young's modulus and dry etching rate of polydimethylsiloxane (pdms)," *Biomedical microdevices*, vol. 21, pp. 1–8, 2019.
- [26] D. Lim, J. W. Lee, B. Gassend, G. E. Suh, M. Van Dijk, and S. Devadas, "Extracting secret keys from integrated circuits," *IEEE Transactions on Very Large Scale Integration (VLSI) Systems*, vol. 13, no. 10, pp. 1200–1205, 2005.
- [27] R. Pappu, B. Recht, J. Taylor, and N. Gershenfeld, "Physical one-way functions," Science, vol. 297, no. 5589, pp. 2026–2030, 2002.
- [28] E. Simpson and P. Schaumont, "Offline hardware/software authentication for reconfigurable platforms," in *Cryptographic Hardware and Embed*ded Systems (CHES), 2006, pp. 311–323.
- [29] M. Majzoobi and F. Koushanfar, "Time-bounded authentication of FPGAs," *IEEE Transactions on Information Forensics and Security*, vol. 6, no. 3-2, pp. 1123–1135, 2011.
- [30] U. Chatterjee, R. Sadhukhan, V. Govindan, D. Mukhopadhyay, R. S. Chakraborty, S. Pati, D. Mahata, and M. M. Prabhu, "PUFSSL: an opensal extension for PUF based authentication," in *Digital Signal Processing (DSP)*, 2018, pp. 1–5.
- [31] S. S. Kumar, J. Guajardo, R. Maes, G. J. Schrijen, and P. Tuyls, "The butterfly PUF: protecting IP on every FPGA," in *Hardware-Oriented* Security and Trust (HOST), 2008, pp. 67–70.

- [32] M. M. Yu, D. M'Raïhi, R. Sowell, and S. Devadas, "Lightweight and secure PUF key storage Using limits of machine learning," in Cryptographic Hardware and Embedded Systems (CHES), 2011, pp. 358–373.
- [33] U. Rührmair, "SIMPL systems as a keyless cryptographic and security primitive." in *Cryptography and Security*. Springer, 2012, pp. 329–354.
- [34] M. Shayan, S. Bhattacharjee, J. Tang, K. Chakrabarty, and R. Karri, "Bio-protocol watermarking on digital microfluidic biochips," *IEEE Trans. Inf. Forensics Secur.*, vol. 14, no. 11, pp. 2901–2915, 2019.
 [35] J. Tang, M. Ibrahim, and K. Chakrabarty, "Randomized checkpoints: A
- [35] J. Tang, M. Ibrahim, and K. Chakrabarty, "Randomized checkpoints: A practical defense for cyber-physical microfluidic systems," *IEEE Design Test*, vol. 36, no. 1, pp. 5–13, 2019.
- [36] L. M. Fidalgo and S. J. Maerkl, "A software-programmable microfluidic device for automated biology," *Lab Chip*, vol. 11, pp. 1612–1619, 2011.
- [37] T. Rey, G. Chagnon, J.-B. Le Cam, and D. Favier, "Influence of the temperature on the mechanical behaviour of filled and unfilled silicone rubbers," *Polymer Testing*, vol. 32, no. 3, pp. 492–501, 2013.
- [38] A. Lau, H. Yip, K. Ng, X. Cui, and R. Lam, "Dynamics of microvalve operations in integrated microfluidics," *Micromachines*, vol. 5, no. 1, p. 50–65, Feb 2014.
- [39] F. R. Hogan, J. Ballester, S. Dong, and A. Rodriguez, "Tactile dexterity: Manipulation primitives with tactile feedback," in *international conference on robotics and automation (ICRA)*, 2020, pp. 8863–8869.